Soft Matter

Dynamic Article Links

Cite this: *Soft Matter*, 2011, **7**, 3155

www.rsc.org/softmatter

PAPER

Coupled oscillations in a 1D emulsion of Belousov–Zhabotinsky droplets†

Jorge Delgado,‡[a] Ning Li,‡[b] Marcin Leda,[a] Hector O. González-Ochoa,[b] Seth Fraden*[b] and Irving R. Epstein[a]

Received 2nd November 2010, Accepted 8th December 2010
DOI: 10.1039/c0sm01240h

We experimentally and computationally study the dynamics of interacting oscillating Belousov–Zhabotinsky (BZ) droplets of ~120 μm diameter separated by perfluorinated oil and arranged in a one-dimensional array (1D). The coupling between BZ droplets is dominated by inhibition and is strongest at low concentrations of malonic acid (MA) and small droplet separations. A microfluidic chip is used for mixing the BZ reactants, forming monodisperse droplets by flow-focusing and directing them into a hydrophobized 100 μm diameter capillary. For samples composed of many drops and in the absence of well defined initial conditions, the anti-phase attractor, in which adjacent droplets oscillate 180° out-of-phase, is observed for strong coupling. When the coupling strength is reduced the initial transients in the phase difference between neighboring droplets persist until the BZ reactants are exhausted. In order to make quantitative comparison with theory, we use photosensitive $Ru(bipy)_3^{2+}$-catalyzed BZ droplets and set both boundary and initial conditions of arrays of small numbers of oscillating BZ droplets with a programmable illumination source. In these small collections of droplets, transient patterns decay rapidly and we observe several more complex attractors, including ones in which some adjacent droplets are in-phase. Excellent agreement between experiment and numerical simulations is achieved.

Introduction

Active matter refers to materials composed of self-propelled agents which continuously consume energy to generate collective motion.[1–3] The field of active matter is young and dominated by theory; lack of model experimental systems that can easily be reproduced and studied by many groups has hampered progress. Developing robust experimental active matter systems is challenging because of the tendency for irreversible processes to degrade the active agents and prevent them from functioning. Biological active matter (*e.g.*, flocks, cytoskeleton) works reliably *in vivo* because of extensive repair mechanisms, which have not been replicated *in vitro*. We present here the first steps towards development of a chemically based active matter experimental system, active emulsions. Collective motion requires two attributes from the active agents: communication and motion. Here we focus solely on the development of communication in active emulsions, leaving the challenge of self-propulsion for the future.[4–6]

Synchronization of a large number of elementary units plays a key role in the functioning of many complex biological and social systems. Examples include quorum sensing in bacteria,[7] ciliary fields,[8,9] cardiac muscle contraction,[10] neural activity and insect behavior.[11,12] Driven entrainment has often been used to induce and to modulate synchronization dynamics.[13–15] As an example of coupled non-linear chemical oscillators, the Belousov–Zhabotinsky (BZ) reaction, the metal-ion-catalyzed oscillatory oxidation of an organic substrate, most commonly malonic acid (MA), by bromate, has become the prototype of non-linear dynamics in chemistry and a preferred system for exploring the dynamics of coupled non-linear oscillators.[16] Micron-sized beads have been employed as BZ reactors, and several strategies have been devised to achieve coupling between these oscillators.[17–19] In these examples, coupling among the oscillators occurs *via* all chemical species; here we restrict the subset of coupling species, in order to promote inhibitory coupling. A problem of particular interest is to determine the attractor(s), *i.e.*, the stable dynamical state(s) to which a system of interacting oscillators spontaneously evolves.

Here we study a linear array of discrete, coupled, non-linear chemical oscillators composed of emulsions of aqueous BZ droplets in oil stored in a capillary in order to form a one-dimensional (1D) array. As demonstrated previously,[20,21] a small subset of the BZ chemicals, an inhibitory component, bromine (Br_2), and an excitatory component, bromine dioxide radical ($BrO_2^{\bullet}$), diffuse from drop to drop through the intervening oil, thereby producing a chemical coupling between drops. Bromine brominates malonic acid, generating bromide and thereby inhibiting the autocatalytic oxidation of the catalyst.[22–24] Since bromine is the principal chemical diffusing between BZ drops, inhibitory coupling dominates. Bromine is produced in a short interval of time during each cycle of the oxidation transition, so each BZ drop that has just undergone an

[a]*Department of Chemistry, Brandeis University, Waltham, MA, 02454-9110, USA*
[b]*Department of Physics, Brandeis University, Waltham, MA, 02454-9110, USA. E-mail: fraden@brandeis.edu*

† Electronic supplementary information (ESI) available: Matlab code used to generate the theoretical results of figures 6–12. See DOI: 10.1039/c0sm01240h

‡ These authors contributed equally to this work.

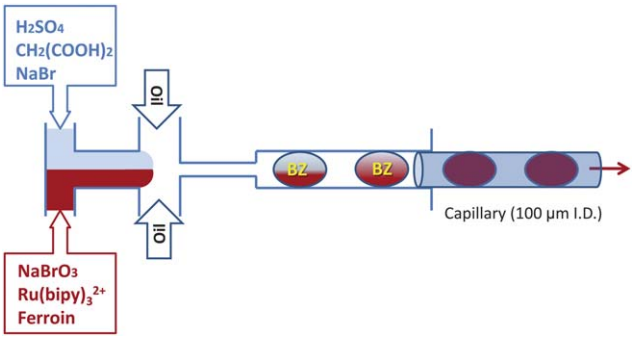

Fig. 1 Schematic drawing of the microfluidic PDMS device drop generator. At left, two different aqueous streams containing complementary reactants of the BZ solution are injected into the drop generator (light blue and red). The streams merge and co-flow down a central channel, meeting two perpendicular oil flows that generate BZ droplets in a nozzle (see Experimental section for details). The co-flow of the BZ solution is preserved immediately after the drops are formed, but complete mixing takes place in less than 1 s. A glass capillary (100 μm ID) was inserted in the PDMS chip a few millimetres downstream from the nozzle to collect the BZ droplets.

oxidation transition emits a pulse of Br_2 that acts to delay the transition of its neighboring drops resulting in the out-of-phase response. Since the system is closed (the BZ reactants are not replenished) after at most 100 oscillations, reactants are consumed substantially, so that oscillations cease as the final equilibrium state is approached. Previous studies[20,21] raise several questions: (1) How reproducible are the "attractors" observed, especially since the patterns found are not true attractors, but are only metastable at best, since the experiments are conducted in a closed system? (2) Pursuing the analogy that each BZ droplet can be thought of as a non-linear oscillator, can we arbitrarily set the initial and boundary conditions of each element of an array of oscillators? (3) How does the number of droplets (oscillators) affect the behavior of the system? (4) Can one vary the coupling strength? (5) Can one control the system by external perturbations, *e.g.*, shifting it from one attractor to another? (6) Are theoretical models able to quantitatively model the observations? Answering these questions is the goal of this paper.

Materials and methods

BZ droplet production in oil by microfluidics

In our experiments, each droplet contains about 1 nL of BZ solution and is separated by a plug of fluorinated oil. A fluorinated surfactant (EA, RainDance Technologies, Lexington, MA, USA) consisting of a PEG–PFPE amphiphilic block copolymer[25] is added to the oil at 2% v/v to prevent the coalescence of the BZ drops. The choice of surfactant is crucial. Bromine reacts with double bonds, and therefore surfactants with unsaturated alkyl tails, such as Span80, are unsuitable because they consume the available bromine, thereby preventing bromine from diffusing between BZ drops.[21] Monodisperse BZ droplets in the fluorinated oil HFE-7500 (3-ethoxy-1,1,1,2,3,4,4,5,5,6,6,6-dodecafluoro-2-trifluoromethyl-hexane, 3M Corp., St Paul, MN, USA) are produced by the use of a polydimethylsiloxane (PDMS) microfluidic device depicted in Fig. 1. This chip has two inlets for injecting equal amounts of complementary components of the aqueous BZ solution into a central channel, where the two BZ reactant streams merge and form a co-flow without mixing. All chemicals are injected at twice the final desired concentration in the BZ droplets according to Table 1. After merging, the BZ co-flow encounters two streams of fluorinated oil entering perpendicularly from both sides. The oil and BZ streams are immiscible and flow into a 50 μm nozzle, which produces droplets by flow-focusing.[26,27] The total flow rate is typically about 1000 μL h^{-1}. It is important to monitor the co-flow and only collect emulsions during conditions when the flow is stable. We place both catalysts in the same co-flow, thereby generating one colored stream and one clear stream, making it simple to visualize the steady state flow that is necessary to ensure that all drops have identical chemical compositions. After their formation, the droplets enter a hydrophobized capillary of 100 μm internal diameter (ID) previously inserted into the microfluidic chip. The experiments cannot be conducted in PDMS devices because bromine is soluble in PDMS, which allows so much bromine to leave the drops that the oscillations cease. Droplets larger than the capillary diameter distort into spherocylinders. The outlet channel of the PDMS chip has a width of 150 μm and height of 40 μm to ensure a snug fit for the glass capillary, which has an outer diameter of 170 μm. The capillaries are hydrophobized using a vacuum chamber in which the capillaries and a small amount of liquid (tridecafluoro-1,1,2,2-tetrahydrooctyl)trichlorosilane are placed. We reduce the pressure in order to evaporate the silane, which enters the capillaries *via* diffusion. The trichlorosilane group of this molecule reacts with the oxygen groups of the silica on the internal glass surface, covering the surface with hydrophobic fluorinated carbon tails.[28] After two hours in the vacuum chamber, which is sufficient for hydrophobizing the capillaries, we remove the capillaries. Air stops the reaction, because oxygen reacts with the chlorosilane groups.

Table 1 Initial concentrations of species in the BZ droplets produced on the microfluidic chip. The solutions of the chemicals injected in channels 1 and 2 were prepared at twice the concentrations given in the table, since each stream undergoes a 1 : 2 (v/v) dilution inside the chip when a BZ droplet is formed

	Chemical	Final concentration in the droplet/mM
Channel 1	Bromate (BrO_3^-)	300
	Ferroin ($Fe(phen)_3^{2+}$)	3
	Tris-bipyridine ruthenium ($Ru(bipy)_3^{2+}$)	0.4
Channel 2	Sulfuric acid (H_2SO_4)	80
	Malonic acid ($CH_2(COOH)_2$)	From 30 to 2800 as described in the text
	Sodium bromide (NaBr)	10

Malonic acid and the chloride salt of tris(2,2′-bipyridyl)ruthenium(II), here referred to as $Ru(bipy)_3^{2+}$, were supplied by Sigma-Aldrich, sulfuric acid and sodium bromate by Fisher, and tris(1,10-phenanthroline)iron(II), here referred to as ferroin, was supplied by Aqua Solutions.

1D BZ droplet observation in capillaries

Capillaries containing identical, equidistant BZ droplets were sealed with commercial epoxy (Hysol® Quick-Cure 5 min epoxy)

on a microscope slide and observed with a CCD camera through a homemade microscope with Köhler illumination. Unless otherwise noted, we observe droplets placed in the central part of the capillary, at least 15 droplets away from the epoxy seal. Typically, more than 100 drops are contained in each capillary. From digital images captured at constant intervals (2–5 s) we extract a single row of pixels per image located on the capillary axis to build the experimental space–time plots presented here. The space–time plots, like the one shown in Fig. 2, are binarized and the intensity is inverted. In the space–time plot, each thin line parallel to the space axis (black in Fig. 2, white in all photographs) corresponds to oxidization of the catalyst from ferroin (iron(II)) to ferriin (iron(III)), which occurs in each cycle of this relaxation oscillation. The regions between the narrow dark lines correspond to intervals during which the reduced form of the catalyst, ferroin (iron(II)), is the dominant species.

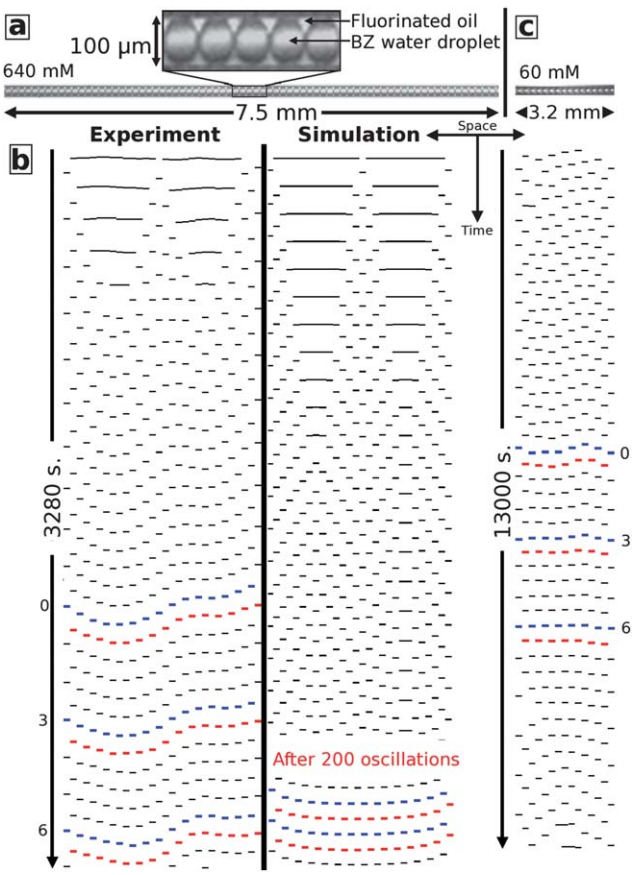

Fig. 2 (a) Upper photograph shows detail of BZ droplets in a 100 μm diameter capillary. Lower photograph shows a section of a capillary containing 75 BZ droplets. (b) Experiment: binarized, intensity-inverted, space–time plot of BZ oscillations of droplets at [MA] = 0.64 M. Space is horizontal; time flows vertically from top to bottom. Each black bar corresponds to the oxidized state of a single drop; white regions correspond to the reduced state. At $t = 0$ (not shown), all droplets are synchronized in the reduced state using external light forcing. An arbitrary reference oscillation is labeled "0" with every odd-indexed drop colored blue and every even-indexed drop colored red. Simulation: space–time plot of a simulation of 30 BZ drops separated by oil. Initial conditions are the same as in experiment (c). Binarized, intensity-inverted, space–time plot of BZ oscillations of 15 droplets at [MA] = 0.060 M in the middle of a large sample. Image of the capillary containing the droplets from which the space–time plot is obtained is presented at the top.

External light forcing

As previously noted, the droplets are loaded with the co-catalyst $Ru(bipy)_3^{2+}$ (0.4 mM). Exposure of the $Ru(bipy)_3^{2+}$ loaded BZ reaction solution to 450 nm light triggers the photochemical production of bromide,[29] inhibiting the BZ oscillations and forcing ferroin into its reduced state. When the light is subsequently turned off, a droplet containing BZ solution begins to oscillate and we assign the phase of the oscillation to be zero at the moment the light is turned off. This phenomenon offers a strategy to externally synchronize and control the droplet state in a programmable way by light. To accomplish this goal, we built the experimental setup shown in Fig. 3, similar to those employed for maskless photolithography purposes.[30–32] Lenses L1 and L2 ($f1 = f2 = 30$ mm) form a Köhler illumination optical path. Ferroin, the catalyst, which also serves as an indicator for the oscillation, has an absorption peak near 510 nm.[33] We accordingly use a cyan LED [Lumiled, LXML-PE01-0050] as a light source for observation and an interference filter centered at 515 nm to narrow the incident wavelength. Therefore the reduced state is dark due to absorbance of the transmitted light and the oxidized state is bright. The projector arm consists of a LCD computer projector (NEC VT800), which uses three 0.63″ LCDs of 1024 × 768 pixels resolution to display color images. Lens L3, a continuous variable zoom lens with a focal distance range of $f = 18.9$ to 22.7 mm, forms a 4× reduced image of the computer projector LCD. For this particular computer projector, we were able to remove the manufacturer's projector lens and remount it with its direction reversed so that instead of magnifying the image located on the three LCDs, the lens (L3) reduces the image. Lens L4 (a discarded 35 mm film Minolta photographic lens, $f = 50$ mm) and the microscope objective (Olympus 4×, RMS4X, $f = 45$ mm) together form an infinite conjugate lens pair through the beam-splitter [Chroma 21000 50/50]. The pair transfers the LCD image formed by L3 onto the sample plane with roughly a 1 : 1 magnification. The tube lens of the objective, lens L5 (Olympus, $f = 180$ mm), and the microscope objective form another infinite conjugate pair lens that transfers the sample image onto the CCD sensor. The contrast ratio between "on" and "off" pixels in these LCD computer projectors is about 180 : 1. A more significant problem is leakage of light through the projector in the off state. In some circumstances this leakage light can influence the experiments, in which case we insert a neutral density filter to lower this background light enough so that it does not affect the period of the BZ oscillations, but still allow enough transmitted light so that when the projector is on there is sufficient light to suppress the BZ oscillation. Typically, to illuminate the samples we use 90 μW intensity of 510 nm wavelength light integrated over the field of view of approximately 8 mm^2. The computer projector has three colors; RGB, each with 8 bits of intensity. To synchronize the BZ reaction we set the R and G values to zero and use B only, because that is the color for which the $Ru(bipy)_3^{2+}$ is most sensitive. Typically the magnification is such that 30 pixels correspond to a drop diameter. When the blue is fully turned on

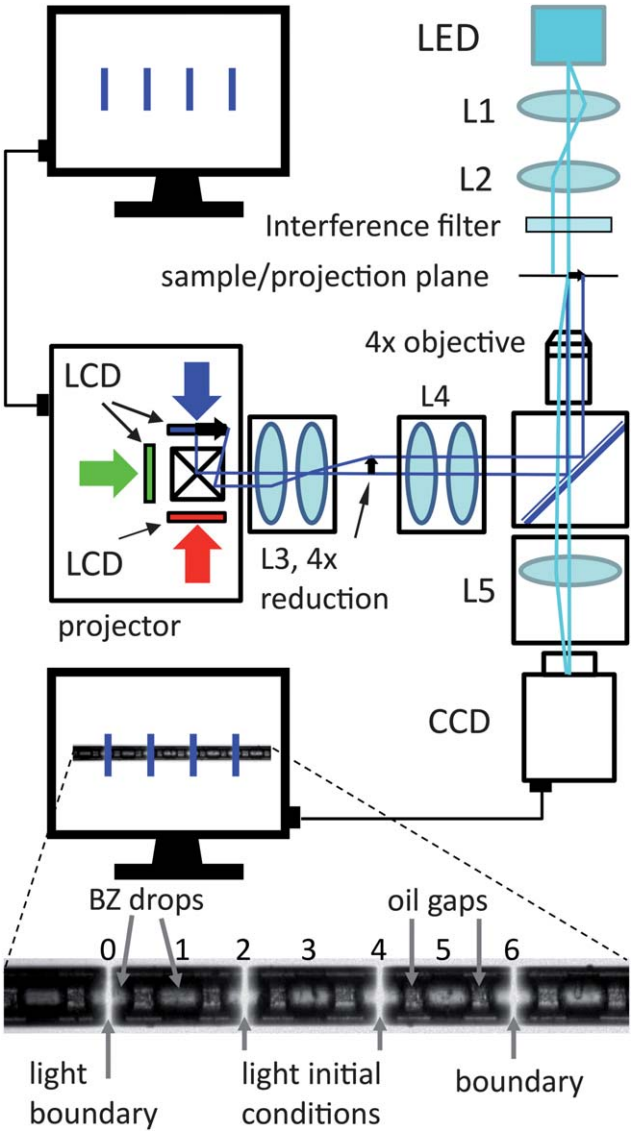

Fig. 3 Optical path for programmable illumination and optical microscope using transmitted light. A consumer electronics computer projector was modified to project an image onto the capillaries containing the BZ microdrops. Programs, such as Powerpoint, were used to create patterned illumination. Photograph: section of a capillary of 100 μm diameter showing 9 BZ drops. The outermost lines of light, labeled "boundary", remain illuminated for the duration of the experiment, suppressing oscillations and thereby isolating the five drops between the light induced boundaries from the rest of the drops in the capillary. To establish initial conditions, the five isolated drops are exposed to light for one oscillation period and another two drops receive additional illumination, labeled "initial condition", to phase shift these two with respect to the other drops.

($B = 255$), the intensity over the entire 8 mm^2 area is 3.6 mW. When the blue is turned off ($B = 0$), light leaks through the LCDs giving an integrated intensity of 20 μW. To synchronize drops, we use patterned illumination with $B = 150$.

This approach allows us to perform spatiotemporal manipulation of the BZ reaction with a spatial resolution of a single drop and a time resolution of ~1 s. In order to minimize the effect on neighboring drops, the intensity of the light is set at the minimal level necessary to suppress oscillation in the illuminated drops. In this way, a localized light pulse on a particular droplet of interest suppresses its oscillation for the duration of illumination, thereby allowing the phase of the oscillator to be set photochemically. This programmable illumination permits the initial phase of each member of a chosen set of droplets to be arbitrarily specified. As described in more detail below, droplets held by constant illumination in the reduced state of the catalyst can act to establish constant chemical "boundary" conditions in a 1D array, so with the use of a programmable computer projector we are able to control both the boundary and initial conditions of a set of coupled non-linear chemical oscillators. Our current set-up allows the simultaneous spatial and temporal illumination of up to 30 droplets individually in a 100 μm capillary. We can image up to 100 droplets with a different lower magnification set-up, but are no longer able to independently illuminate individual droplets. When we study capillaries with 100 droplets we illuminate the entire capillary with uniform, bright light in order to set all the drops in-phase.

Results and discussion

Out-of-phase attractors: high and low [MA] regimes

In previous studies,[20,21] the anti-phase attractor was reported to be the most common pattern for emulsions of BZ droplets in oil in a 1D configuration under conditions dominated by inhibitory coupling. It was concluded[20] that for the BZ conditions used in this paper (Table 1) the coupling between drops was mainly due to the diffusion of the inhibitory species Br_2 through the oil. This conclusion was based on the experimental observation that addition of a bromine scavenger eliminated coupling effects and the fact that the theoretical results were almost identical with and without inclusion of the diffusive coupling of the excitatory species $BrO_2^{\bullet}$, especially for [MA] > 0.2 M. In contrast, at low MA, the results indicate the increasing importance of excitatory coupling in addition to strong inhibitory coupling; investigations of this regime will be the subject of a subsequent study. Utilizing the concentrations of the BZ reactants listed in Table 1, we obtain out-of-phase inhibitory patterns using monodisperse droplets with diameters ranging between 100 and 220 μm when the droplets are uniformly spaced, with gaps between drops ranging from near-contact to 130 μm. In this section we present experiments on 1D arrays of approximately 100 droplets interacting along the axis of a 100 μm diameter hydrophobized capillary. Approximately 75 droplets are imaged simultaneously, and beyond the field of vision there are at least 15 more droplets on each side before the sealed end of the capillary. We will describe the typical behavior of these systems for several different concentrations of malonic acid, [MA].

In Fig. 2a an image of a segment of a capillary containing 100 drops with [MA] = 0.64 M is shown. Fig. 2b shows the space–time plot of this system after illumination with a bright light that initializes all the drops in-phase in the reduced state of ferroin at the beginning of the experiment. When the drops first transition from the reduced to the oxidized state, displayed as a black bar in Fig. 2b, most start in-phase. Our numerical simulations (see Appendix) reveal that during the short oxidized portion of the

oscillation the Br_2 concentration in each drop is high. At this moment in the oscillation cycle the drop is less susceptible to having its phase shifted by the addition of Br_2 diffusively transferred from a neighboring drop than at a later time in the drop's cycle. With time, Br_2 is removed through bromination of malonic acid, after which the oxidation transition can reoccur. Notice in Fig. 2b that a few drops transition with a delay. Focus on the isolated delayed drop in the middle of the space–time plot in Fig. 2b, which emits Br_2 during the oxidation transition. If this transition is sufficiently delayed, then it occurs when $[Br_2]$ in the neighboring drops has reached a relatively low value, and these drops will receive a sufficient dose of Br_2 from the emitter to delay their next oxidation transition. In turn, these new delayed drops influence their in-phase neighbors, and the number of in-phase drops decreases monotonically.

In Fig. 2b the time of an arbitrary oxidation transition on the left side of the space–time plot is labeled "0". We pick the left-most drop and color in blue the oxidation transition that occurs at time "0". Then we label in blue the oxidized state of its second nearest neighbor that is closest in time to its oxidation transition and in this manner continue painting transitions of every other drop blue until we reach the right hand side of the space–time plot. In this way we construct a "wave front" of the oxidized state. We color in red the transition of the drop that is second from the left that is closest in time to the first blue drop and continue proceeding from left to right until each second nearest neighbor drop is labeled red. If the drops were in an attractor where every other drop had a phase difference of 0.5 periods with its two nearest neighbors, then the blue and red wave fronts would be straight and separated in time by exactly half a period. Fig. 2b also shows a simulation of a capillary containing 30 drops with [MA] = 0.64 M. In the simulation, calculated using a modified version of a previously used extension of the FKN model,[34] described in the Appendix, the length of the BZ drops is equal to 200 microns with a vanishing oil gap (10^{-4} μm), to model the experimental case of drops in contact. The outermost drop at each end is modeled to be held at a constant illumination, which prevents those drops from oscillating, effectively forming constant concentration boundary conditions. Only the remaining 28 drops, which are not illuminated and therefore can oscillate, are shown in the space–time plot. The simulations are done on "open" systems in which the principal chemical reagents that feed the BZ reaction are held constant (see Appendix for details), so the reaction can oscillate forever. Initially, three drops, the nearest neighbor to each boundary drop and one drop in the middle of the system, are set 180° out-of-phase with all the other drops. With each transition, the out-of-phase drops cause neighboring in-phase drops to delay their oxidation transition, leading to the conversion of the initial in-phase to the out-of-phase pattern. It takes about 200 oscillations for the transients to die out and a final, stable oscillatory pattern to be reached. In an infinite system the final state would consist of neighboring drops oscillating 180° out-of-phase with each other, and in the space–time plot the oxidation transitions of the even (red) and odd (blue) indexed drops would form straight lines offset by half a period. In contrast, the final simulated steady state oscillatory pattern in Fig. 2b is gently curved as a consequence of the influence of the boundaries propagating into the center of the sample. Later we show that, for these conditions, samples must contain more than 40 drops in order for boundary conditions to be negligible.

Since the coupling between drops is diffusive, the time for transients to decay grows as the square of the number of drops. The experimental system is over three times larger than the simulated one so we predict that it will take well over 1000 oscillations for transients to decay in an experimental system of 100 drops. Since the closed experimental system oscillates at most 100 times before the reaction goes to completion, samples of 100 drops that are started in-phase will never reach the steady oscillatory pattern.

Fig. 2c shows an experimental space–time plot of a capillary filled with [MA] = 0.060 M. The first several oscillations that occurred after turning off external illumination to synchronize the drops were not recorded. In contrast to the case of high malonic acid, the conversion from the initial in-phase to final out-of-phase pattern is rapid. Simulations reflect this trend.

To quantitatively analyze the oscillatory patterns in the experimental linear array of BZ drops, we define the period of the i^{th} droplet, τ_i, as the time between two consecutive oxidation transitions and assume the phase of the droplet to increase linearly in time from 0 to 1 between each pair of transitions. Throughout the text and in the figures of this paper, we calculate the phase difference between two droplets i and j ($\Delta\phi_{i-j}$) by measuring the time difference between the n^{th} oxidation transition of the i^{th} drop and the n^{th} oxidation transition of the j^{th} drop. If the difference is negative, we repeatedly add +1 to the value until the difference is positive. If the difference is greater than 1, we take the result modulo 1.

We take the experimental data shown in Fig. 2b and c and calculate the normalized distribution of $\Delta\phi$ – modulo 1 (binned in intervals of 0.05), using 14 pairs of adjacent droplets, shown in Fig. 4. To lower the noise in the distribution of phase-differences, we plot $\langle\Delta\phi_{\text{Dist}}\rangle$, obtained by averaging the normalized distribution of $\Delta\phi$ over three consecutive oscillatory periods. For each of the experiments shown in Fig. 2b and c we arbitrarily choose a particular oxidation transition as the origin for the phase measurement. These reference times are about 10–15 oscillations after the synchronizing illumination is turned off.

Since our system is closed and must therefore ultimately reach a situation in which all droplets are in the same non-oscillatory equilibrium state, τ and $\Delta\phi_{\text{Dist}}$ change in time. However, in most cases we observe that, after a short initial transient phase, there is an interval in which $\Delta\phi_{\text{Dist}}$ is nearly stationary for many periods of oscillation. We consider the corresponding state to represent an "attractor" of the system. Fig. 4a and b present $\langle\Delta\phi_{\text{Dist}}\rangle$ for [MA] = 0.060 M and 0.64 M, respectively, corresponding to the space–time plots of Fig. 2c and b. For [MA] = 0.060 M (Fig. 2c), the distribution of phase differences (Fig. 4a), $\langle\Delta\phi_{\text{Dist}}\rangle$, is relatively narrow and exhibits a pronounced maximum around $\Delta\phi$ = 0.5 during ~6 oscillatory periods, from 6000 to 9500 s starting about 10 oscillations after the cessation of the synchronizing illumination. During the time interval corresponding to oscillations 9–15, the average period of all the droplets, $\langle\tau\rangle$, remains almost constant at 550 s and the standard deviation of $\langle\Delta\phi_{\text{Dist}}\rangle$, σ, is small, meaning that the droplets are well entrained. Because of the narrowness of $\langle\Delta\phi_{\text{Dist}}\rangle$ and the nearly constant period $\langle\tau\rangle$, we can consider the system strongly coupled in an anti-phase attractor during these six periods. $\langle\Delta\phi_{\text{Dist}}\rangle$ broadens slightly with

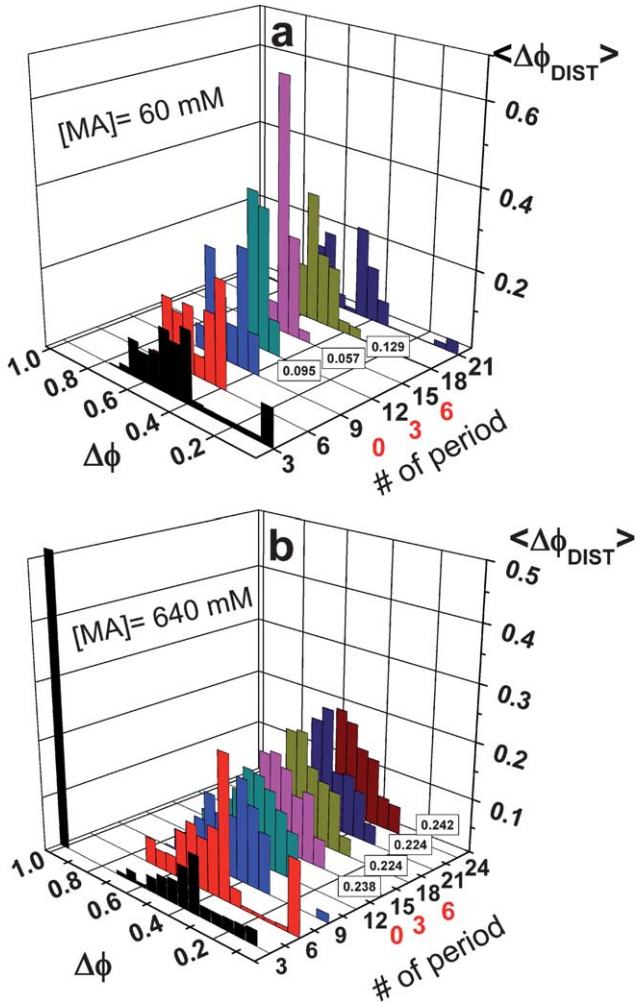

Fig. 4 (a) Normalized phase-difference distribution ($\langle\Delta\phi_{\mathrm{Dist}}\rangle$) between nearest neighbor droplets for [MA] = 60 mM as a function of oscillation number after synchronization by light. Data are obtained from periods numbered 0–6 in the space–time plot in Fig. 2c. $\langle\Delta\phi_{\mathrm{Dist}}\rangle$ was averaged over consecutive time intervals of 3 periods. Boxed numbers next to the $\langle\Delta\phi_{\mathrm{Dist}}\rangle$, labeled as 12, 15 and 18, are the widths of the distribution. (b) Normalized phase-difference distribution ($\langle\Delta\phi_{\mathrm{Dist}}\rangle$) between nearest neighbor droplets for [MA] = 640 mM as a function of oscillation number after synchronization by light obtained from periods numbered 0–6 in the space–time plot in Fig. 2b.

time in this interval, but the $\Delta\phi$ components in $\langle\Delta\phi_{\mathrm{Dist}}\rangle$ between 0.45 and 0.55 always comprise at least 60% of the distribution. After 15 periods, $\langle\tau\rangle$ and σ start to increase in this closed system, and the strong coupling among droplets is lost. We speculate that this behavior is due to the irreversible consumption of chemical reagents.

In contrast, for [MA] $\geq$ 0.20 M the fraction of droplet pairs with $0.45 < \Delta\phi < 0.55$ is much lower, as observed in Fig. 4b for [MA] = 0.64 M with the corresponding space–time plot shown in Fig. 2b. $\langle\Delta\phi_{\mathrm{Dist}}\rangle$ is still centered near $\Delta\phi = 0.5$, but the distribution at high malonic acid (Fig. 4b) is significantly broader than $\langle\Delta\phi_{\mathrm{Dist}}\rangle$ at low malonic acid (Fig. 4a). As shown in Fig. 4b, $\langle\Delta\phi_{\mathrm{Dist}}\rangle$ remains stationary for 10 periods beginning from period 12, although the oscillation period $\langle\tau\rangle$ gradually decreases in time from $\langle\tau\rangle = 170$ s to $\langle\tau\rangle = 160$ s. We conclude that, even in our

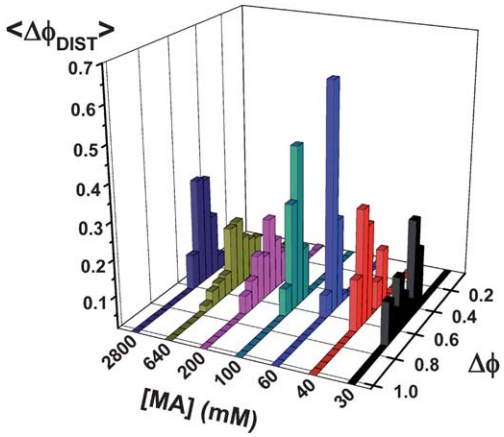

Fig. 5 Normalized time-averaged phase-difference distribution ($\langle\Delta\phi_{\mathrm{Dist}}\rangle$) obtained from measurements of 15 droplets in the center of capillaries containing about 100 drops for several malonic acid concentrations. The measurements begin about 10 periods after synchronization by light and are obtained during the most stationary behavior, corresponding to the minimum standard deviation in the period of oscillation of the drops. The variation in the widths of the distributions for MA > 30 mM reflects transient behavior more than systematic trends.

closed system, this regime produces stable out-of-phase patterns, albeit the oscillators appear to be weakly coupled, since the spread in phase differences between neighboring drops is high. We observe this weak coupling behavior from [MA] = 0.20 M up to 2.8 M. The manifestation of weak coupling in the space–time plot of Fig. 2b is the wavy form of the oxidation transition wavefronts in contrast to the straight wavefronts in Fig. 2c for strong coupling.

By focusing on the time intervals where $\langle\Delta\phi_{\mathrm{Dist}}\rangle$ is nearly stationary, we can compare the out-of-phase patterns obtained under different chemical conditions. Fig. 5 shows experimental phase difference distributions, $\langle\Delta\phi_{\mathrm{Dist}}\rangle$, for several [MA] measured about 10 oscillations after the drops are synchronized with exposure to light. Note that in all cases the transients in the phase difference between drops have not disappeared. Simulations indicate that for [MA] > 30 mM the width of the distribution is dominated by this transient behavior; the steady state interdrop phase difference in the center of these large linear arrays is predicted to be precisely 0.5. The trend of increasing width of the distribution with increasing [MA] suggests that at high [MA] the system takes a longer time to attain the anti-phase state. Experiments and computational modeling both suggest a decrease in the inhibitory coupling *via* bromine when [MA] increases. Weakened coupling at high [MA] explains why drops take longer to synchronize into a steady state oscillatory pattern.

In another simulation, shown in Fig. 6, we study 40 drops and start the drops with 180° out-of-phase initial conditions. The space–time pattern evolves without producing phase defects and the system evolves to a steady-state oscillatory pattern after about 100 cycles. If the number of drops is large enough, then for adjacent drops far enough away from the boundaries, $\Delta\phi = 0.5$ as shown in Fig. 6. The range of influence of the boundaries is a function of [MA]. At low values of [MA], the effect of the boundaries is less than at higher [MA]. We obtained the same results with two different boundary conditions, one

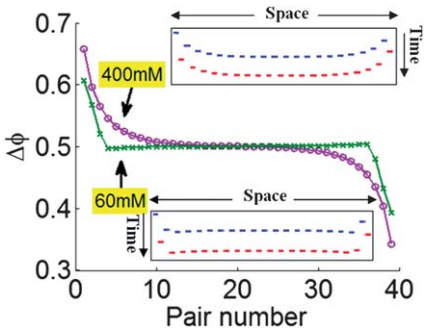

Fig. 6 Simulation of the phase difference between 40 BZ drops of 200 μm diameter separated by gaps of 50 μm of oil for high (400 mM) and low (60 mM) concentrations of malonic acid. The drops on the boundary are given sufficient light to prevent oscillation; $k(I) = 10^{-4}$ [s^{-1}] for high [MA] and 10^{-3} for low [MA]. The insets contain space–time plots from which the phase differences were derived. Blue represents odd numbered drops and red even numbered drops. One oxidation transition is shown for each of the drops.

corresponding to drops exposed to just enough light to suppress oscillations and one corresponding to sealed walls at each end of the array. The interpretation of these results is that in the limit of large 1D arrays of BZ emulsions the attractor consists of nearest neighbors oscillating precisely half a period out-of-phase. This out-of-phase attractor is the only stable attractor we observed in simulations in 1D. It is possible in simulations to obtain other attractors, but they are unstable in the sense that if a small perturbation in the phase difference between oscillators is introduced, then the oscillators evolve towards the out-of-phase attractor.

In both the experiments and the simulations, the coupling is strongest for low [MA] and close spacing of drops. It is possible to develop some intuition regarding the observed trends based on eqn (23) in the Appendix. This equation describes the change of the inhibitor concentration, [Br_2], in the BZ drops. If we focus solely on the terms involving Br_2, then a continuum version of eqn (23) is given by the reaction–diffusion equation $\frac{\partial u}{\partial t} = -k_{\text{eff}}u + D\nabla^2 u$ with $k_{\text{eff}} = k_6 + k_7 = 10$ [s^{-1}] + 29 [M^{-1} s^{-1}] [MA]. From dimensional analysis, one can define a characteristic reaction–diffusion length over which one drop interacts with another as $\lambda \approx \beta\sqrt{D/k_{\text{eff}}}$ with β a numerical constant. Weak coupling occurs when the center to center separation between drops, $L = (a + b)/2$, with a the drop diameter and b the length of the oil gap (see Fig. 13), is larger than λ. Physically, increasing the separation between drops weakens the coupling, because the time for Br_2 to diffuse between drops scales as L^2. Chemically, Br_2 brominates malonic acid, and so with increasing [MA] the bromination rate also increases, thereby decreasing the amount of Br_2 available to diffuse between drops and produce chemical coupling. This chemistry is incorporated in the effective rate constant k_{eff} *via* k_7 so that increasing [MA] decreases λ.

Behavior of small groups of droplets isolated by illumination

We are ultimately interested in establishing whether the system of coupled oscillators has well-defined attractors and, if so, we would like to enumerate them and characterize their basins of attraction. However, as seen in the previous section, there are several experimental problems in dealing with arrays containing a large number of drops. First, the results presented above suggest that for large droplet arrays at higher [MA], transients in the phase difference between oscillators persist beyond the time for the BZ reaction to cease oscillation. Second, at high [MA] the coupling is weak and the system has a tendency to drift, making it difficult to set initial conditions of the oscillators with a brief perturbation. Third, near [MA] = 0.060 M, where the coupling appears strongest, the anti-phase attractor is very stable and the basins of attraction of other patterns may be quite small. Finally, the approximation that [MA] remains constant breaks down at low [MA]. For [MA] < 30 mM, the BZ drops cease to oscillate after only a few periods and the drops enter a Turing state in which some are permanently in the oxidized state and others in the reduced state, and often pairs of in-phase oscillators are observed. The solution to this set of problems is to study small groups of drops at intermediate [MA] with well established initial and boundary conditions.

We first focus on groups of 3–5 droplets for [MA] between 0.20 M and 0.40 M, where the phase of the droplets can easily be shifted using external light forcing as described in the Experimental section. Typically, the capillaries are filled with 100 droplets, but the droplets of interest are isolated from the rest of the capillary by two non-oscillatory droplets, which are fixed in the reduced state by the applied illumination, which provides symmetric boundary conditions. Additionally, by illuminating the droplets in the group of interest with a selected spatiotemporal pattern, we can place the system in a desired initial state, as illustrated in Fig. 3. We also attempt to reproduce our experimental results with computer simulations, which are described in the Appendix. All simulations in this section are done with the length of the BZ droplet, $a = 200$ μm, length of the oil gap, $b = 50$ μm, and [MA] = 400 mM. In this section we adopt a particular notation to describe the phase relationship between adjacent drops, whereby the phase of a drop is indicated by a lower case letter. For example, if we have four drops with every other drop having the same phase, we refer to this situation as an "a–b–a–b" array. One important point is that, since the system is closed, it necessarily drifts away from the attractor that would exist in an open system. Thus in the experiments described below we employ simulations of open systems to identify the underlying attractor observed in experiment.

Results with 3 drops. The only pattern we found with 3 droplets is the "a–b–a" attractor, in which the phase difference of the two outer droplets with the drop in the center is $\phi_b - \phi_a = \Delta\phi \approx 0.6$. This measurement is clearly distinguishable from the case when the drops are 180° out-of-phase with $\Delta\phi = 0.5$. This pattern is reached independent of the initial phases of the drops. As an example, Fig. 7a shows that an initial "a–a–b" pattern is unstable and eventually evolves to the stable "a–b–a" pattern. We also explored a variety of other initial conditions, including the symmetric "a–a–a" state. Fig. 7b shows the experimental phase difference $\Delta\phi$ between each drop and a reference drop as a function of time extracted from the space–time data in Fig. 7a. Note that the first 5×10^3 s of the experiment are shown in the space–time plot of Fig. 7a, while 11×10^3 s of the experiment are analyzed in Fig. 7b. The phase difference is calculated between

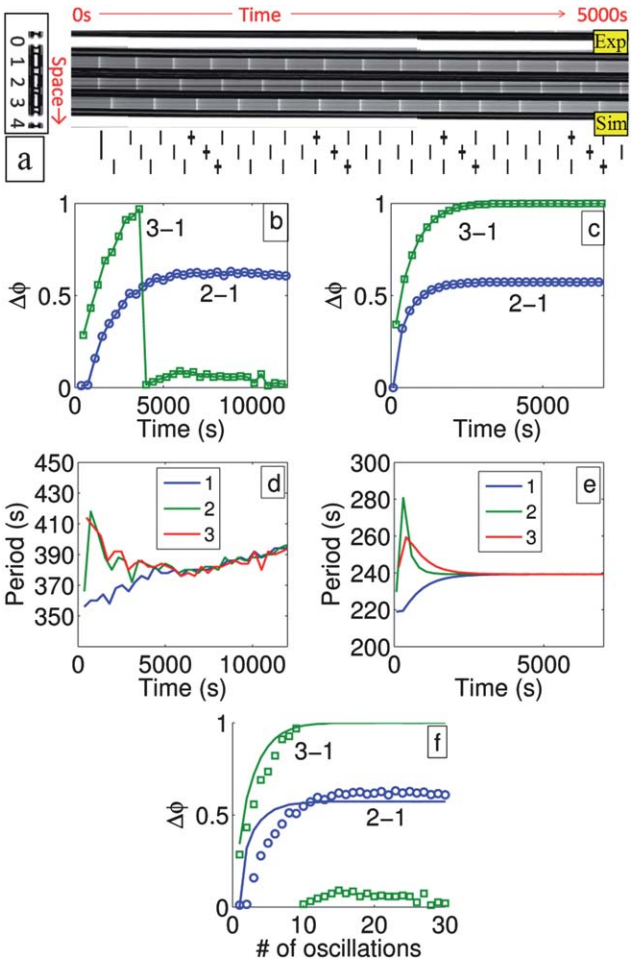

Fig. 7 Temporal evolution of three BZ drops isolated by constant illumination from the rest of the capillary; symmetric attractor. (a) Exp: space–time plot of 5 drops in the center of a 100 μm diameter capillary entirely filled with BZ drops. [MA] = 320 mM. Average BZ droplet length, $a = 219$ μm (±1%); lengths of oil gaps between the oscillating BZ drops are 62 μm and 36 μm. Inset: photograph of the 5 BZ drops. Drops 0 and 4 are illuminated with constant light in order to isolate drops 1, 2 and 3 from the rest of the capillary. Initially drops 1 and 2 oscillate in phase while drop 3 is delayed. Sim: simulation of the 5 drops with same chemical and initial conditions as the experiment. The "+" symbol indicates oxidation transitions for every fourth oscillation of each drop. (b) Experimental phase difference (modulo 1) between pairs of drops, *i.e.* 2 − 1 (blue curve) means the phase difference between drop 2 and 1. Note that phase differences of 1 and 0 are equivalent. (c) Corresponding simulated phase difference. (d) Experimental and (e) simulated periods of oscillation for each droplet. (f) Experimental and calculated phase difference as a function of the number of oscillations.

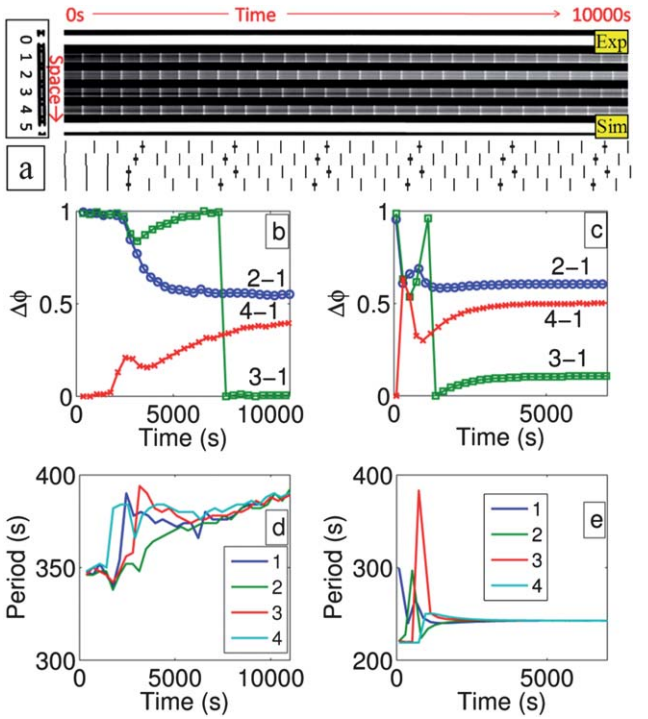

Fig. 8 Temporal evolution of four BZ drops; asymmetric attractor. (a) Exp: space–time plot of 6 drops. [MA] = 320 mM. BZ drop length, $a = 218$ μm (±1%), oil gap length, $b = 46$ μm (±7%). Inset: photograph of the 6 BZ drops. Drops 0 and 5 are illuminated with constant light in order to isolate drops 1 to 4, which are initially synchronized by light and evolve to an out-of-phase pattern. Sim: simulation of the 6 drops. Every fourth oscillation is marked by a "+". (b) Experimental and (c) corresponding simulated phase difference. (d) Experimental and (e) simulated periods of oscillation for each droplet.

drops that have oscillated the same number of times. For example, even though at late times in the space–time plot of Fig. 7a the first and third drops undergo nearly simultaneous oxidation transitions (vertical white bars), drop 1 has undergone approximately one more oscillation than drop 3 so their phase difference is nearly 1, not 0. In Fig. 7b, c, and f each symbol corresponds to the occurrence of an oxidation transition, so from inspection of the figures we see that it takes 10 oscillations for drops 1 and 3 to become synchronized. This symbol convention is employed in Fig. 8–12 as well. Numbering the three droplets of interest from top to bottom, we observe that drop 1 initially has a shorter period than drops 2 and 3 (Fig. 7d), enabling it to drift out-of-phase with drop 2 and in phase with drop 3. Once the stable "a–b–a" pattern is established, the initially disparate periods of the drops become identical, though τ drifts monotonically in time as previously described at high [MA] (Fig. 7d). Fig. 7c and e show simulations corresponding to Fig. 7b and d, respectively. Note that, in both the experiment and the simulation, after the initial transient has died out the observed out-of-phase attractor of the center drop has $\Delta\phi \approx 0.6$, which differs from the ideal anti-phase behavior ($\Delta\phi = 0.5$) as a result of interactions with the boundary. Simulations demonstrate that the phase shift caused by the boundary can take on a wide range of values depending on the chemical composition of the BZ solution and the light intensity. The simulations shown in Fig. 6 suggest that boundary effects extend about 10 drops into the array for high [MA].

Since the simulations do not take into account the consumption of the reactants, once synchrony is obtained, the oscillation period in Fig. 7e remains constant rather than slowly increasing as in Fig. 7d. We suggest that the collective drift in the experimental period, beginning at $t = 5000$ s in Fig. 7d, is a consequence of the system being closed. Another inadequacy in the model is that the calculated periods of oscillation do not quantitatively match the experimental periods. The inability of the

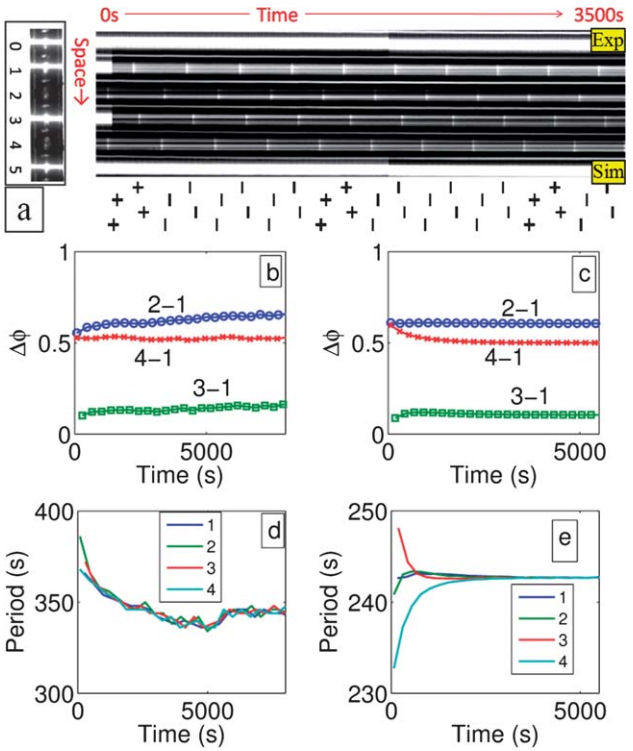

Fig. 9 Temporal evolution of four BZ drops; asymmetric attractor. (a) Exp: space–time plot of 6 drops. [MA] = 380 mM. $a = 116$ μm (±3%), $b = 17$ μm (±11%). Inset: photograph of the 6 BZ drops. Drops 0 and 5 are illuminated with constant light. Drops 1 and 3 are illuminated for about 300 seconds. With light perturbation, the 4 drops start with an out-of-phase pattern and reach a similar out-of-phase pattern as Fig. 8, but much faster. Sim: simulation of the 6 drops. Every fourth oscillation is marked by a "+". (b) Experimental and (c) simulated phase difference. (d) Experimental and (e) simulated periods of oscillation for each droplet.

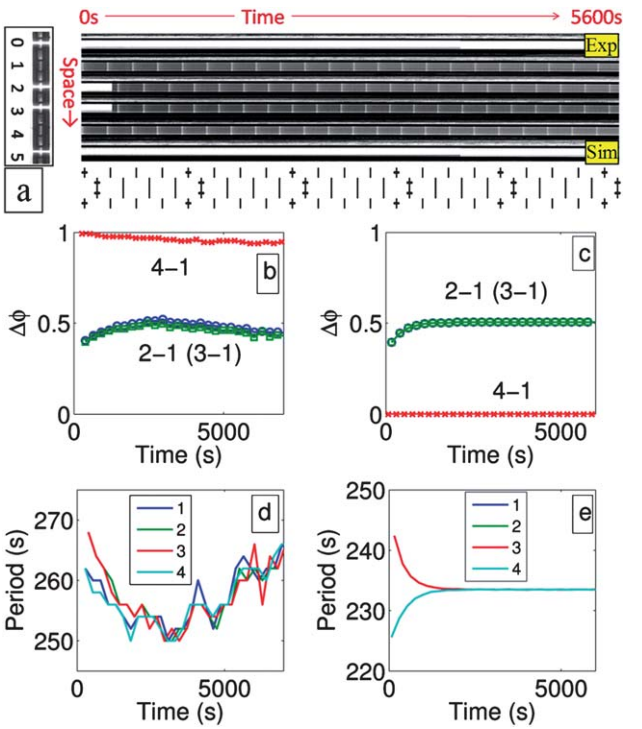

Fig. 10 Temporal evolution of four BZ drops; symmetric attractor. (a) Exp: space–time plot of 6 drops. [MA] = 380 mM. $a = 194$ μm (±2%), $b = 129$ μm (±6%). Inset: photograph of the 6 BZ drops. Drops 0 and 5 are illuminated with constant light. Drops 2 and 3 are illuminated for about 300 s. Sim: simulation of the 6 drops. Every fourth oscillation is marked by a "+". (b) Experimental phase difference. (c) Simulated phase difference. (d) Experimental and (e) simulated periods of oscillation for each droplet.

FKN model to accurately calculate the period of the BZ oscillation has been discussed previously.[35] However, Fig. 7f shows that experiment and simulation agree when we plot the phase difference as a function of the non-dimensional period (*i.e.*, the number of oscillations). Note in Fig. 7f that $\Delta\phi = 0$ is equivalent to $\Delta\phi = 1$.

Results with 4 drops. For four droplets, we are able to obtain two attractors by light manipulation: "a–b–a′–b′" as shown in Fig. 8, 9 and 11 and "a–b–b–a" as shown in Fig. 10. In Fig. 8, an initially synchronized in-phase system ("a–a–a–a") drifts out-of-phase, but the ideal out-of-phase "a–b–a–b" attractor seen in theory to occur in the center of a large sample (Fig. 6), with $\phi_a = 0$ and $\phi_b = 0.5$, does not develop in the four drop case because of the influence of the boundary conditions (or constant production of Br^-) created by the constant illumination of drops 0 and 5. The resulting stable attractor, shown in the simulation of Fig. 8c, is composed of four drops whose phases measured with respect to drop 1 are given by $(\phi_1, \phi_2, \phi_3, \phi_4) = (0.0, 0.6, 0.1, 0.5)$, which is subtly different from the ideal out-of-phase attractor of $(\phi_1, \phi_2, \phi_3, \phi_4) = (0.0, 0.5, 0.0, 0.5)$. In the experiment, Fig. 8b, we observe $(\phi_1, \phi_2, \phi_3, \phi_4) = (0.0, 0.55, 0.0, 0.4)$. Experiment and simulation differ by drops 2, 3 and 4 having phase differences of ~0.1 with respect to drop 1.

We can reach the attractor observed in Fig. 8 more quickly by changing the initial condition using patterned illumination, as seen in Fig. 9, where the initial conditions are $(\phi_1, \phi_2, \phi_3, \phi_4) = (0.0, 0.55, 0.1, 0.53)$. The simulation very rapidly reaches a steady state attractor corresponding to $(\phi_1, \phi_2, \phi_3, \phi_4) = (0.0, 0.6, 0.1, 0.5)$, and the experimental phases are quite close: $(\phi_1, \phi_2, \phi_3, \phi_4) = (0.0, 0.62, 0.12, 0.52)$.

To obtain the "a–b–b–a" attractor, we use light to phase-shift the two middle droplets with respect to the outer droplets to obtain the following initial conditions, $(\phi_1, \phi_2, \phi_3, \phi_4) = (0.0, 0.4, 0.4, 0.0)$, as shown in Fig. 10. The two middle droplets start to oscillate after the light is removed, and they remain in-phase. The experimental $\Delta\phi$ drifts slowly. For the simulation, shown in Fig. 10c, the phase difference between inner and outer drops is 0.5 yielding the symmetric attractor, $(\phi_1, \phi_2, \phi_3, \phi_4) = (0.0, 0.5, 0.5, 0.0)$, which, to within slow temporal drifts, is consistent with experiment.

If we again initialize a 4-drop system by phase shifting the inner two drops with respect to the outer two drops, as in Fig. 10, but this time impose a slight phase difference between the two interior drops to have initial conditions $(\phi_1, \phi_2, \phi_3, \phi_4) = (0.0, 0.55, 0.53, 0.0)$, we see in Fig. 11 that initially the system reaches the "a–b–b–a" attractor, but then jumps to the same "a–b–a′–b′" attractor shown in Fig. 8 and 9 with $(\phi_1, \phi_2, \phi_3, \phi_4) = (0.0, 0.6, 0.1, 0.5)$. Again, to within some slight temporal drift, experiment

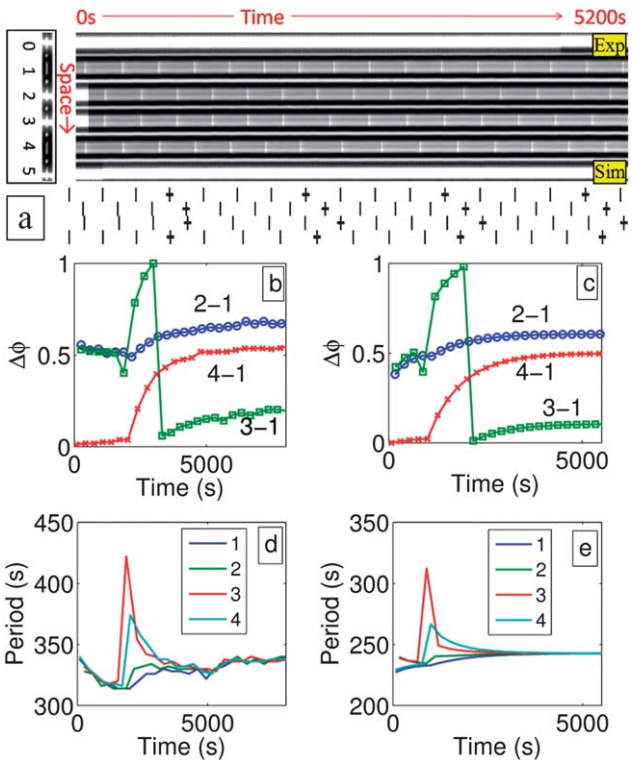

Fig. 11 Temporal evolution of four BZ drops; asymmetric attractor. (a) Exp: space–time plot of 6 drops. [MA] = 380 mM. $a = 109$ μm (±3%), $b = 15$ μm (±12%). Inset: photograph of the 6 BZ drops. Drops 0 and 5 are illuminated with constant light. Drops 2 and 3 are illuminated for about 300 s. The four drops start with a symmetric attractor, as in Fig. 10, but evolve to the same out-of-phase attractor as in Fig. 8 and 9 after a few oscillations. Sim: simulation of the 6 drops. Every fourth oscillation is marked by a "+". (b) Experimental and (c) simulated phase difference. (d) Experimental and (e) simulated periods of oscillation for each droplet.

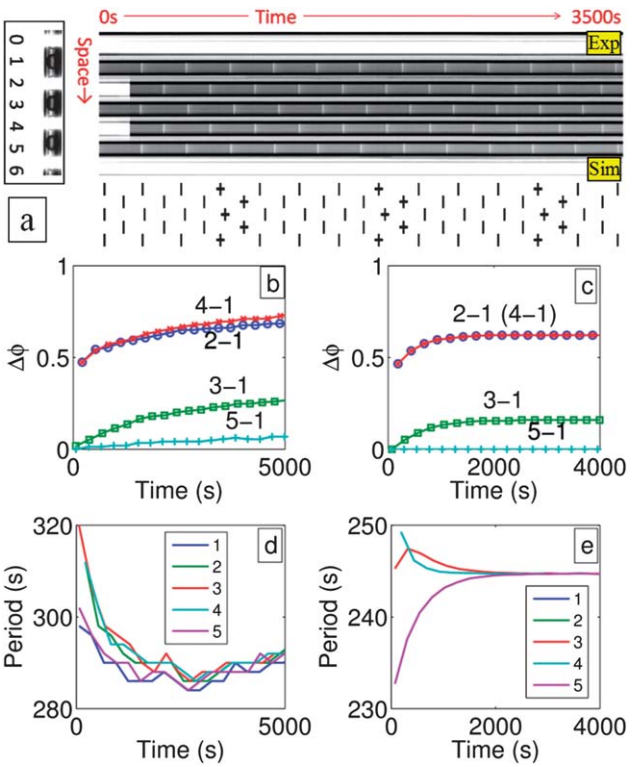

Fig. 12 Temporal evolution of five BZ drops; symmetric attractor. (a) Exp: space–time plot of 7 drops. [MA] = 210 mM. $a = 135$ μm (±1%), $b = 48$ μm (±15%). Inset: photograph of the 7 BZ drops. Drops 0 and 6 are illuminated with constant light. Drops 2 and 4 are illuminated for about 300 s so that the 5 drops start with an out-of-phase pattern. Sim: simulation of the 7 drops. Every fourth oscillation is marked by a "+". (b) Experimental phase difference. (c) Simulated phase difference. (d) Experimental and (e) simulated periods of oscillation for each droplet. Simulated drops 1 and 5 have equal periods, as do drops 2 and 4.

and simulation agree. The "a–b–a′–b′" attractor has a much larger basin of attraction than the "a–b–b–a" attractor.

For the system consisting of four drops, we study the temporal evolution for four different initial conditions. In each case we model the time dependence using the FKN model described in the Appendix. The agreement between simulation and experiment of the temporal evolution of the transient initial state towards the stable attractor shown in the space–time plots and phase-difference plots is excellent. We note that there are no adjustable parameters. The only changes from case to case are the initial conditions, which are chosen to match the experiment. The agreement between theory and experiment is almost quantitative; the one discrepancy is in the period of oscillation, for which the experimental period is between 1.25 and 1.5 times longer than the simulated period. The shortcomings of the FKN model with respect to period have been discussed in the literature.[35] We find two attractors for the four drop system. The one with phase pattern (0.0, 0.6, 0.1, 0.5) seen in Fig. 8 and 9, and 11 approaches the "ideal" anti-phase pattern, where each drop is 0.5 oscillations out-of-phase with its neighbors, as the number of drops becomes large. As the boundary conditions are symmetric, we expected the stable attractor to be symmetric, but instead the stable attractor is asymmetric with the pattern "a–b–a′–b′". We did observe a symmetric attractor, $(\phi_1, \phi_2, \phi_3, \phi_4) = (0.0, 0.5, 0.5, 0.0)$, shown in Fig. 10, whose equivalent we did not observe in experiments with larger numbers of drops. We define the width of the basin of attraction of the symmetric attractor as the magnitude of the maximum initial phase difference between the two middle drops ($\Delta\phi_{32}$) for which the "a–b–b–a" attractor is observed. Given this definition of phase, the basin of attraction could range from $0 < \Delta\phi_{32} < 0.5$. Within our experimental resolution, we were unable to measure the width of the basin of attraction of the symmetric attractor observed in Fig. 10. However, in Fig. 11 we set an upper bound on the basin of attraction; $\Delta\phi_{32} < 0.55–0.53 = 0.02$. We cannot conclude that the symmetric attractor, (0.0, 0.5, 0.5, 0.0), is unstable, but we established that the basin of attraction of the symmetric attractor is much smaller than the basin of attraction of the asymmetric attractor, a–b–a′–b′.

Results with 5 drops. For five droplets, the only stable attractor we find is the "a–b–a′–b–a" pattern with phases $(\phi_1, \phi_2, \phi_3, \phi_4, \phi_5) = (0.0, 0.6, 0.1, 0.6, 0.0)$. This pattern is shown in Fig. 12. It is close to, but different in an experimentally significant way from the ideal out-of-phase pattern expected for an infinite array, where adjacent drops have a phase difference of 0.5.

In general, the experimental attractors are less stable than the corresponding simulated attractors. The consumption of chemical species during the experiment causes changes in the period of oscillation, but the drops largely remain synchronized and this only produces a small steady drift in $\Delta\phi$ compared to the simulations. In all cases, the simulated periods of the drops in the systems composed of 4 or 5 drops are systematically greater than the experimental periods by up to 50%, as noted previously.[35] Nonetheless, the simulated patterns of phase differences, including transient responses to initial conditions, agree qualitatively with the experimental ones.

Conclusion

Emulsions introduce a new length scale, the drop separation (L), to the BZ system, with two regimes of behavior: strong and weak coupling, depending on whether or not the reaction–diffusion length (λ) is greater (strong) or less (weak) than the drop separation. For the conditions we study, emulsions confined to one dimension, inhibition due to inter-drop diffusion of Br_2 causes neighboring drops to oscillate out-of-phase with each other. In experiments on large numbers of drops in a linear array at high concentrations of malonic acid, we measure transient phase defects that take a long time to anneal, indicative of weak chemical coupling. In contrast, at low malonic acid, the transients anneal quickly. Simulations bear out this observation and also indicate that the boundaries influence the phase differences between oscillators. The influence of the boundaries is a function of malonic acid; the boundary influence is greater at high malonic acid, corresponding to weak coupling between oscillators. In order to study interacting BZ droplets systematically, we developed a programmable illumination system that allows the setting of both boundary and initial conditions. We studied the behavior of groups of 3, 4 and 5 drops. The attractors are predominantly out-of-phase as a consequence of the inhibitory coupling, but are modified in non-trivial ways by the boundary conditions. In the case of 4 drops, a second attractor, reflecting the symmetry of the system, is observed. The simulations for the small drop system are in very good agreement with experiment with no adjustable parameters. To realize our goal of creating a BZ-based active matter system, we plan to investigate emulsions in two-dimensions, develop open systems, extend the conditions to include excitatory coupling, study synchronization *via* temporally modulated light, create chemically heterogeneous drops, and introduce mechano-chemical coupling between the BZ reaction and a gel embedded in the emulsion drop.

Appendix: the model for the simulations

To model each BZ drop we begin with the standard FKN model[23,24]

$$\mathrm{HBrO_2 + Br^- + H^+ \rightarrow 2HOBr} \qquad k_1 = 2 \times 10^6\ [\mathrm{M^{-2}\ s^{-1}}]h \tag{1}$$

$$\mathrm{BrO_3^- + Br^- + 2H^+ \rightarrow HBrO_2 + HOBr} \qquad k_2 = 2[\mathrm{M^{-3}\ s^{-1}}]\ h^2A \tag{2}$$

$$\mathrm{2HBrO_2 \rightarrow BrO_3^- + HOBr + H^+} \qquad k_3 = 3000\ [\mathrm{M^{-1}\ s^{-1}}] \tag{3}$$

$$\mathrm{BrO_3^- + HBrO_2 + H^+ \rightarrow 2BrO_2^\bullet + H_2O} \qquad k_4 = 42\ [\mathrm{M^{-2}\ s^{-1}}]\ hA \tag{4}$$

$$\mathrm{HOBr + Br^- + H^+ \rightarrow Br_2 + H_2O} \qquad k_5 = 5 \times 10^9\ [\mathrm{M^{-2}\ s^{-1}}]\ h \tag{5}$$

$$\mathrm{Br_2 + H_2O \rightarrow HOBr + Br^- + H^+} \qquad k_6 = 10\ [\mathrm{s^{-1}}] \tag{6}$$

$$\mathrm{Br_2 + MA \rightarrow BrMA + Br^- + H^+} \qquad k_7 = 29\ [\mathrm{M^{-1}\ s^{-1}}]\ m \tag{7}$$

$$\mathrm{HOBr + MA \rightarrow BrMA + H_2O} \qquad k_8 = 9.3\ [\mathrm{M^{-1}\ s^{-1}}]\ m \tag{8}$$

$$\mathrm{2BrO_2^\bullet + H_2O \rightarrow BrO_3^- + HBrO_2 + H^+} \qquad k_r = 2 \times 10^8\ [\mathrm{M^{-1}\ s^{-1}}] \tag{9}$$

$$\mathrm{BrO_2^\bullet + Fe(phen)_3^{2+} + H^+ \rightarrow HBrO_2 + Fe(phen)_3^{3+}} \qquad k_{red} = 5 \times 10^6\ [\mathrm{M^{-1}\ s^{-1}}] \tag{10}$$

$$\mathrm{Fe(phen)_3^{3+} + BrMA \rightarrow Fe(phen)_3^{2+} + Br^- + ox1} \qquad k_9 = 1\ [\mathrm{M^{-1}\ s^{-1}}]\ B \tag{11}$$

$$\mathrm{Fe(phen)_3^{3+} + MA \rightarrow Fe(phen)_3^{2+} + ox2} \qquad k_{10} = 0.05\ [\mathrm{M^{-1}\ s^{-1}}]\ m \tag{12}$$

where the concentrations of protons, $[H^+] = h$, bromate, $[BrO_3^-] = A$, malonic acid, $[MA] = m$, and bromomalonic acid, $[BrMA] = B = 0.1m$, are taken as constants, and $x = [HBrO_2]$, bromide, $y = [Br^-]$, $p = [HOBr]$, $w = [BrO_2^\bullet]$ in the BZ drop, $r = [BrO_2^\bullet]$ in the oil, $u = [Br_2]$ in the BZ drop, $s = [Br_2]$ in the oil, $c = [Fe(phen)_3^{2+}]$, reduced form of the catalyst, and $z = [Fe(phen)_3^{3+}]$, oxidized form of the catalyst, are variables. While experimentally we use two different catalytic species, $Fe(phen)_3^{2+}$ and $Ru(bipy)_3^{2+}$, in our simulation we disregard this distinction and consider only one photosensitive catalyst represented by $c(z)$ in its reduced (oxidized) form. ox1 and ox2 refer to oxidation products of BrMA and MA. All concentrations are in molar units.

For the photosensitive Ru(II) complex as a catalyst, we add the additional reactions (see eqn (13)–(15) of Vanag and Epstein[34]).

$$\mathrm{Ru(bipy)_3^{2+}} + h\nu \rightarrow \mathrm{Ru(bipy)_3^{2+*}}\ k(I) = 10^{-3}\text{–}10^{-4}\ \mathrm{s^{-1}} \quad (13)$$

$$\mathrm{Ru(bipy)_3^{2+*}} + \mathrm{BrMA} + \mathrm{H^+} \rightarrow \mathrm{Ru(bipy)_3^{3+}} + \mathrm{Br^-} + \text{products}\ k_C \quad (14)$$

$$\mathrm{Ru(bipy)_3^{2+*}} \rightarrow \mathrm{Ru(bipy)_3^{2+}}\ k_d \quad (15)$$

The corresponding set of ordinary differential equations is

$$\mathrm{d}x/\mathrm{d}t = -k_1xy + k_2y - 2k_3x^2 - k_4x + k_rw^2 + k_{red}wc \quad (16)$$

$$\mathrm{d}y/\mathrm{d}t = -k_1xy - k_2y - k_5yp + k_6u + k_7u + k_9z + k(I)cB/(b_C + B) \quad (17)$$

$$\mathrm{d}z/\mathrm{d}t = k_{red}wc - k_9z - k_{10}z + k(I)cB/(b_C + B) \quad (18)$$

$$\mathrm{d}p/\mathrm{d}t = 2k_1xy + k_2y + k_3x^2 - k_5yp + k_6u - k_8p \quad (19)$$

$$\mathrm{d}u/\mathrm{d}t = k_5yp - k_6u - k_7u \quad (20)$$

$$\mathrm{d}w/\mathrm{d}t = 2k_4x - 2k_rw^2 - k_{red}wc \quad (21)$$

$$\mathrm{d}c/\mathrm{d}t = -k_{red}wc + k_9z + k_{10}z - k(I)cB/(b_C + B) \quad (22)$$

where $b_C = k_d/k_C = 0.05$ M. The effect of the photosensitive Ru(II) catalyst is incorporated in the last term of eqn (17), (18), and (22) and is derived from eqn (13), (14), and (15) with the assumption that the excited catalyst, $c = \mathrm{Ru(bipy)_3^{2+*}}$, is in steady-state, *i.e.* $\mathrm{d}c/\mathrm{d}t = 0$[34] in eqn (13)–(15), but $\mathrm{d}c/\mathrm{d}t \neq 0$ in eqn (22).

Non-polar species such as Br_2 (the inhibitor) and $BrO_2^{\bullet}$ (the activator) can diffuse through the oil from one BZ droplet to its neighbor; thus adjacent droplets are coupled. To simulate the coupling, we add diffusion terms for Br_2 and $BrO_2^{\bullet}$ to their reaction equations. The diffusion terms are governed by Fick's first law, $J = -D\frac{\partial u}{\partial x}$ and mass conservation, $\frac{\partial u}{\partial t} = -\frac{\partial J}{\partial x}$. Eqn (23) is an example of a reaction–diffusion equation, $\partial_t u = D\nabla^2 u + R(u)$, where $R(u)$ contains all the reaction terms, *i.e.*, the right hand side of eqn (20). The modification of the FKN model to take into account the diffusive flux of Br_2 and $BrO_2^{\bullet}$ between adjacent BZ and oil drops is:

$$\mathrm{d}u_n/\mathrm{d}t = k_5y_np_n - k_6u_n - k_7u_n + 2D[s_{n-1,n} + s_{n,n+1} - 2P_Bu_n]/[a(a + b)] \quad (23)$$

$$\mathrm{d}s_n/\mathrm{d}t = 2D[P_B(u_n + u_{n+1}) - 2s_{n,n+1}]/[b(a + b)] \quad (24)$$

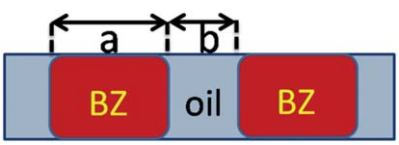

Fig. 13 Geometry of part of the capillary with BZ droplets. We approximate the shape of droplets to be cylindrical. The length along the capillary of a BZ droplet is *a* and oil droplet is *b*.

$$\mathrm{d}w_n/\mathrm{d}t = 2k_4x_n - 2k_rw_n^2 - k_{red}w_nc_n + 2D[r_{n-1,n} + r_{n,n+1} - 2P_Rw_n]/[a(a + b)] \quad (25)$$

$$\mathrm{d}r_n/\mathrm{d}t = 2D[P_R(w_n + w_{n+1}) - 2r_{n,n+1}]/[b(a + b)] \quad (26)$$

where $D = 10^{-5}\ \mathrm{cm^2\ s^{-1}}$ is an estimated diffusion coefficient used for both Br_2 and $BrO_2^{\bullet}$, u_n denotes $[Br_2]$ in the aqueous phase in droplet n, $s_{n,n+1}$ denotes $[Br_2]$ in the oil phase between droplets n and $n + 1$, $P_B = 2.5$ is a spectroscopically measured partition coefficient for Br_2 at the fluorinated oil/water interface, $P_R = 1$ is an estimated partition coefficient for $BrO_2^{\bullet}$, a and b are the lengths along the capillary of the BZ droplets and the oil in between, respectively, as shown in Fig. 13. As we treat the droplets in our model as cylindrical with constant cross-sectional area A, a/b is the volume ratio of the water and oil phases. The number of Br_2 molecules in a drop of volume V_{drop} is ΔN. The derivation of eqn (23)–(26) proceeds by discretizing Fick's Law and the conservation law. At equilibrium, the ratio of concentration of $[Br_2]$ in adjacent oil and BZ drops would be $P_B = s^*/u^*$. Any difference from this partition coefficient drives a diffusive flux between oil and BZ drops:

$$J = -D\frac{\Delta u}{\Delta x} = -D\frac{\Delta u}{L} = D\left(\frac{s - uP_B}{(a + b)/2}\right)$$
$$J = \frac{\Delta N}{\Delta tA} = \frac{\Delta uV_{drop}}{\Delta tA} = \frac{\Delta ua}{\Delta t} \Rightarrow \frac{\Delta u}{\Delta t} = 2D\left[\frac{s - uP_B}{a(a + b)}\right] \quad (27)$$

The derivation of eqn (24)–(26) proceeds similarly.

The simulation mimics the experimental arrangement. For example, to simulate a 3 droplet experiment with light-suppressed boundaries and light perturbation in the middle droplet, we run a 5 droplet simulation with the first and the last droplets continuously exposed to enough light to suppress oscillations in these drops, and we apply light to the middle droplet for a brief initial interval. The initial conditions are: $x_0 = 10^{-6}$ M, $y_0 = 5 \times 10^{-5}$ M, $c_0 = 0.003$ M, and the rest of the species starts from zero concentrations. The Matlab code is available as a supplement. We use the Matlab function ode15s (multistep solver of variable order based on the numerical differentiation formulas) to solve the system of coupled differential equations with a relative tolerance of 10^{-8} and an absolute tolerance of 10^{-9}.

Acknowledgements

This work was supported by the National Science Foundation (CHE-0615507 and MRSEC DMR-0820492). We thank Michael Heymann and Sathish Akella for generous assistance in experiment and discussion.

References

1 F. Julicher, K. Kruse, J. Prost and J. F. Joanny, Active behavior of the cytoskeleton, *Phys. Rep.*, 2007, **449**, 3–28.
2 J. Toner, Y. H. Tu and S. Ramaswamy, Hydrodynamics and phases of flocks, *Ann. Phys. (Amsterdam, Neth.)*, 2005, **318**, 170–244.
3 E. Karsenti, Self-organization in cell biology: a brief history, *Nat. Rev. Mol. Cell Biol.*, 2008, **9**, 255–262.
4 J. Shen, S. Pullela, M. Marquez and Z. D. Cheng, Ternary phase diagram for the Belousov–Zhabotinsky reaction-induced mechanical oscillation of intelligent PNIPAM colloids, *J. Phys. Chem. A*, 2007, **111**, 12081–12085.

5 R. Yoshida, Self-oscillating gels driven by the Belousov–Zhabotinsky reaction as novel smart materials, *Adv. Mater.*, 2010, **22**, 3463–3483.
6 V. V. Yashin and A. C. Balazs, Chemomechanical synchronization in heterogeneous self-oscillating gels, *Phys. Rev. E: Stat., Nonlinear, Soft Matter Phys.*, 2008, **77**, 046210.
7 E. P. Greenberg, Quorum sensing in gram-negative bacteria, *Am. Soc. Microbiol. News*, 1997, **63**, 371–377.
8 A. Vilfan and F. Julicher, Hydrodynamic flow patterns and synchronization of beating cilia, *Phys. Rev. Lett.*, 2006, **96**, 058102.
9 B. Guirao and J. F. Joanny, Spontaneous creation of macroscopic flow and metachronal waves in an array of cilia, *Biophys. J.*, 2007, **92**, 1900–1917.
10 L. Glass, Synchronization and rhythmic processes in physiology, *Nature*, 2001, **410**, 277–284.
11 S. C. Pratt, Quorum sensing by encounter rates in the ant *Temnothorax albipennis*, *Behav. Ecol.*, 2005, **16**, 488–496.
12 T. D. Seeley, P. K. Visscher and K. M. Passino, Group decision making in honey bee swarms, *Am. Sci.*, 2006, **94**, 220–229.
13 S. H. Strogatz, *Nonlinear Dynamics and Chaos: With applications to Physics, Biology, Chemistry, and Engineering*, Perseus Books Publishing, 1994.
14 A. Pikovsky, M. Rosenblum, and J. Kurths, *Synchronization—A Universal Concept in Nonlinear Sciences*, Cambridge University Press, 2001.
15 T. M. Massie, B. Blasius, G. Weithoff, U. Gaedke and G. F. Fussmann, Cycles, phase synchronization, and entrainment in single-species phytoplankton populations, *Proc. Natl. Acad. Sci. U. S. A.*, 2010, **107**, 4236–4241.
16 I. R. Epstein and J. A. Pojman, An Introduction to Nonlinear Chemical Dynamics, *Oscillations, Waves, Patterns, and Chaos*, Oxford University Press, 1998.
17 A. F. Taylor, M. R. Tinsley, F. Wang, Z. Y. Huang and K. Showalter, Dynamical quorum sensing and synchronization in large populations of chemical oscillators, *Science*, 2009, **323**, 614–617.
18 T. Okano, A. Kitagawa and K. Miyakawa, Array-enhanced coherence resonance and phase synchronization in a two-dimensional array of excitable chemical oscillators, *Phys. Rev. E: Stat., Nonlinear, Soft Matter Phys.*, 2007, **76**, 046201.
19 T. Okano and K. Miyakawa, Feedback-controlled dynamics in a two-dimensional array of active elements, *Phys. Rev. E: Stat., Nonlinear, Soft Matter Phys.*, 2009, **80**, 046215.
20 M. Toiya, H. O. Gonzalez-Ochoa, V. K. Vanag, S. Fraden and I. R. Epstein, Synchronization of chemical micro-oscillators, *J. Phys. Chem. Lett.*, 2010, **1**, 1241–1246.
21 M. Toiya, V. K. Vanag and I. R. Epstein, Diffusively coupled chemical oscillators in a microfluidic assembly, *Angew. Chem., Int. Ed.*, 2008, **47**, 7753–7755.
22 L. Hegedus, M. Wittmann, Z. Noszticzius, S. H. Yan, A. Sirimungkala, H. D. Forsterling and R. J. Field, HPLC analysis of complete BZ systems. Evolution of the chemical composition in cerium and ferroin catalysed batch oscillators: experiments and model calculations, *Faraday Discuss.*, 2001, **120**, 21–38.
23 R. J. Field, R. M. Noyes and E. Koros, Oscillations in chemical systems. 2. Thorough analysis of temporal oscillation in bromate–cerium–malonic acid system, *J. Am. Chem. Soc.*, 1972, **94**, 8649–8664.
24 R. M. Noyes, R. J. Field and E. Koros, Oscillations in chemical systems. 1. Detailed mechanism in a system showing temporal oscillations, *J. Am. Chem. Soc.*, 1972, **94**, 1394–1395.
25 C. Holtze, A. C. Rowat, J. J. Agresti, J. B. Hutchison, F. E. Angile, C. H. J. Schmitz, S. Koster, H. Duan, K. J. Humphry, R. A. Scanga, J. S. Johnson, D. Pisignano and D. A. Weitz, Biocompatible surfactants for water-in-fluorocarbon emulsions, *Lab Chip*, 2008, **8**, 1632–1639.
26 S. L. Anna, N. Bontoux and H. A. Stone, Formation of dispersions using "flow focusing" in microchannels, *Appl. Phys. Lett.*, 2003, **82**, 364–366.
27 T. M. Squires and S. R. Quake, Microfluidics: fluid physics at the nanolitre scale, *Rev. Mod. Phys.*, 2005, **77**, 977–1026.
28 V. Depalma and N. Tillman, Friction and wear of self-assembled trichlorosilane monolayer films on silicon, *Langmuir*, 1989, **5**, 868–872.
29 R. Toth and A. F. Taylor, The tris(2,2 ′-bipyridyl)ruthenium-catalysed Belousov–Zhabotinsky reaction, *Prog. React. Kinet. Mech.*, 2006, **31**, 59–115.
30 K. Itoga, M. Yamato, J. Kobayashi, A. Kikuchi and T. Okano, Cell micropatterning using photopolymerization with a liquid crystal device commercial projector, *Biomaterials*, 2004, **25**, 2047–2053.
31 J. D. Musgraves, B. T. Close and D. M. Tanenbaum, A maskless photolithographic prototyping system using a low-cost consumer projector and a microscope, *Am. J. Phys.*, 2005, **73**, 980–984.
32 T. Naiser, T. Mai, W. Michel and A. Ott, Versatile maskless microscope projection photolithography system and its application in light-directed fabrication of DNA microarrays, *Rev. Sci. Instrum.*, 2006, **77**, 063711.
33 D. T. Newcombe, T. J. Cardwell, R. W. Cattrall and S. D. Kolev, An optical redox chemical sensor based on ferroin immobilised in a Nafion® membrane, *Anal. Chim. Acta*, 1999, **401**, 137–144.
34 V. K. Vanag and I. R. Epstein, A model for jumping and bubble waves in the Belousov–Zhabotinsky–aerosol OT system, *J. Chem. Phys.*, 2009, **131**, 104512.
35 T. Turanyi, L. Gyorgyi and R. J. Field, Analysis and simplification of the GTF model of the Belousov–Zhabotinsky reaction, *J. Phys. Chem.*, 1993, **97**, 1931–1941.